Electromagnetic edge plasma turbulence simulations in varying beta conditions

Raffael Düll [1]

[1] CNRS M2P2

TSVV1 annual meeting

Garching b. München - October 8, 2025

The SOLEDGE3X Framework

- Fluid solver for the drift-reduced Braginskii equations [Bufferand et al. 2022]

- Conservation equations for density, parallel momentum, and energy
- Finite-volume method, implicit–explicit time integration
- Perpendicular dynamics dominated by drifts:

$$\beta = \frac{p}{p_{\mathrm{mag}}} = \frac{enT}{B^2/2\mu_0}$$

$$\mathbf{v}_\perp = \underbrace{\mathbf{v}_E}_{\text{electric}} + \underbrace{\mathbf{v}_*}_{\text{diamagnetic}} + \underbrace{\mathbf{v}_p}_{\text{polarization}}$$

- Assumptions:
  - Higher collisionality at low temperatures
  - Static poloidal field at low-β
  - Quasineutrality
- Fixed axisymmetric magnetic equilibrium:
  - Meshing aligned to flux surfaces, domain extends edge $\rightarrow$ wall

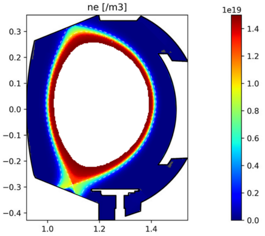

Fixed diffusion coefficients

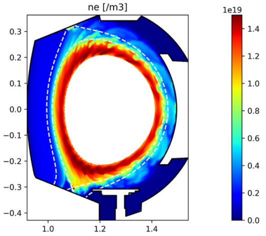

Drift-driven transport

Ingredients for Electromagnetism

Starting point: Electrostatic non-adiabatic electron response to fluctuations [Bufferand et al. 2022]

MAGNETIC INDUCTION

Variation of the magnetic vector potential in the parallel electric field:

$$E_{\|} = -\nabla_{\|}\Phi - \partial_t A_{\|}$$

where $A_{\|}$ is known from Ampère's law:

$$\nabla_{\perp}^2 A_{\|} = \mu_0 j_{\|}$$

FLUTTER

Fluctuations of the magnetic field induced by $A_{\|}$.

Consequence of the definition of the magnetic vector potential:

$$\nabla \times \mathbf{A} = \mathbf{B}$$

ELECTRON INERTIA

Non-zero electron mass: the non-adiabatic electron response to fluctuations is delayed by an inertial term

$$\frac{m_e}{n_e e^2} \partial_t j_{\|} + \nabla \cdot (j_{\|} \mathbf{v}_j)$$

Full Electromagnetic Model Equations

Flutter $\mathbf{b} = \mathbf{b}_{eq} + \mathbf{b}_{pert}$

Mass conservation: $\partial_t n_i + \nabla \cdot \left(n_i \left(\mathbf{v}_\perp + v_\| \boxed{\mathbf{b}}\right)\right) = S_{n,i}$

Parallel momentum conservation: $m_i \partial_t \Gamma_i + m_i \boldsymbol{\nabla} \cdot \left(\Gamma_{\|,i} \left(\mathbf{v}_\perp + v_\| \boxed{\mathbf{b}}\right)\right) = Z_i n_i E_\| - \boldsymbol{\nabla} \cdot \left(\nu_\| \boxed{\mathbf{b}} \cdot \boldsymbol{\nabla} v_\|\right) + R_{\|,i} + S_{\Gamma,i}$

Electron energy conservation: $\partial_t \varepsilon_e + \nabla \cdot \left((\varepsilon_e + p_e)\left(\mathbf{v}_\perp + v_\| \boxed{\mathbf{b}}\right)\right) = \left(\mathbf{v}_\perp + v_\| \boxed{\mathbf{b}}\right) \cdot (-n_e \mathbf{E} + \mathbf{R}_e - \boldsymbol{\nabla} \cdot \boldsymbol{\Pi}_e) - \boldsymbol{\nabla} \cdot \left(\kappa_\| \boxed{\mathbf{b}} \cdot \boldsymbol{\nabla} T_e\right) + S_{\varepsilon,e}$

Ion energy conservation: $\partial_t \varepsilon_i + \nabla \cdot \left((\varepsilon_i + p_i)\left(\mathbf{v}_\perp + v_\| \boxed{\mathbf{b}}\right)\right) = \left(\mathbf{v}_\perp + v_\| \boxed{\mathbf{b}}\right) \cdot (Z_i n_i \mathbf{E} + \mathbf{R}_i - \boldsymbol{\nabla} \cdot \boldsymbol{\Pi}_i) - \boldsymbol{\nabla} \cdot \left(\kappa_\| \boxed{\mathbf{b}} \cdot \boldsymbol{\nabla} T_i\right) - \boldsymbol{\nabla} \cdot \left(\nu_\| \boxed{\mathbf{b}} \cdot \boldsymbol{\nabla} v_\|^2\right) + S_{\varepsilon,i}$

Vorticity equation: $\boldsymbol{\nabla} \cdot \left[\frac{m_i n_i}{B^2} \partial_t \boldsymbol{\nabla}_\perp \Phi\right] - \boldsymbol{\nabla}\left(j_\| \mathbf{b}\right) = \boldsymbol{\nabla} \cdot \left(\mathbf{j}_{\nabla B} + \mathbf{j}_\Pi + \mathbf{j}_\pi\right) - \boldsymbol{\nabla} \cdot \left[\frac{m_i}{e Z_i B^2} \partial_t \boldsymbol{\nabla}_\perp p_i\right]$

Electron inertia

Ohm's law: $\eta_\| j_\| + \boxed{\frac{m_e}{n_e e^2}\left(\partial_t j_\| + \boldsymbol{\nabla} \cdot \left[j_\| \mathbf{v}_j\right]\right)} = -\boxed{\mathbf{b}} \cdot \boldsymbol{\nabla} \Phi - \boxed{\partial_t A_\|} + T_e \boxed{\mathbf{b}} \cdot \boldsymbol{\nabla} \log(n_e) + 1.71 \boxed{\mathbf{b}} \cdot \boldsymbol{\nabla} T_e$

Ampère's law: $\boxed{\boldsymbol{\nabla} \cdot \boldsymbol{\nabla}_\perp A_\| + \mu_0 j_\|} = 0$

Magnetic induction

Sheath boundary conditions:

- Particle flux $\Phi_{n,BC}$ from the Bohm–Chodura condition $v_{BC} > c_s$
- Energy flux $\Phi_{\varepsilon,BC} = \gamma T \Phi_{n,BC}$ with the sheath transmission coefficient γ
- Sheath current $j_{BC} = Z_i e \Phi_{n,BC}\left(1 - e^{\Lambda - \phi/T_e}\right)$ with the potential drop Λ
- Magnetic vector potential $A_{BC} = 0$

Implicit Resolution of the Electromagnetic Vorticity Equation

Resistive, Alfvénic and electron inertia occur at fast time scales $\rightarrow$ Implicit resolution in a coupled system

Electrostatic

$$\left(D_\perp \partial_t \nabla_\perp^2 + D_\| \nabla_\|^2\right)(\phi) = \dots$$

with: $D_\perp = \frac{m_i n_i}{B^2}$ and $D_\| = \frac{1}{\eta_\|}$

High anisotropy !

Electromagnetic

$$\begin{pmatrix} D_\perp \partial_t \nabla_\perp^2 + D_\| \nabla_\|^2 & \beta_0 D_\| \partial_t \nabla_\| \\ -D_\| \nabla_\| & \beta_0 D_\| \partial_t - \nabla_\perp^2 \end{pmatrix} \begin{pmatrix} \phi \\ A_\| \end{pmatrix} = \dots$$

with: $D_\perp = \frac{m_i n_i}{B^2 \delta_t}$ and $D_\| = \frac{1}{\eta_\| + m_e/(n_e \delta_t)}$

The parallel current $j_\|$ can be decoupled

$\rightarrow$ updated in a second step

- **Electron inertia** improves the condition for low resistivity $\eta_\|$
  - parallel diffusion coefficient on ϕ: $1/\eta \rightarrow 1/(\eta + m_e/(n_e \delta_t))$.
- **Magnetic induction** deteriorates the matrix condition for low β_0.
- The **condition number** of the electromagnetic system worsens twice as fast with the perpendicular resolution.

Calculating Electromagnetic Flutter

Assume small perturbations of the magnetic field:

$$\mathbf{B} = \mathbf{B}_{eq} + \mathbf{B}_{\text{pert}}$$

From the value of the toroidal fluctuation field $\tilde{A}_{\parallel}$:

$$\mathbf{B}_{\text{pert}} = \nabla \times \left(\mathbf{b}_{eq} A_{\parallel}\right) - \mathbf{b}_{eq} \times \nabla A_{\parallel}$$

Why toroidal fluctuations of $\tilde{A}_{\parallel}$?

The toroidal component of $A_{\parallel}$ overlaps with the poloidal flux function Ψ to generate the magnetic configuration

- Risk of accounting parts of the Grad–Shafranov shift twice

$$\tilde{A}_{\parallel} = A_{\parallel} - \langle A_{\parallel} \rangle_{\varphi}$$

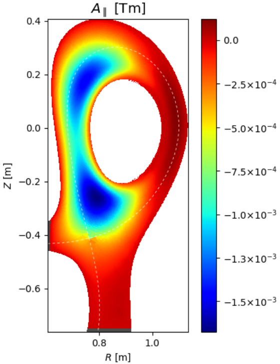

(a) *full field $A_{\parallel}$*

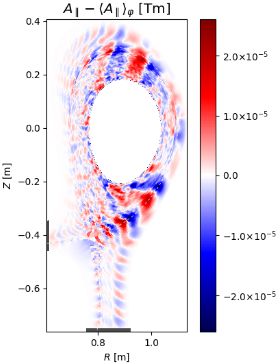

(b) *Toroidal fluctuations $\tilde{A}_{\parallel}$*

Figure 1: *Parallel magnetic vector potential on a TCV configuration*

Linear analysis of drift-wave instabilities

- ExB drift advection coupled with Ampère's law and electron inertia in an isothermal setting
- Imposed parallel modes $k_{\|} = 0.6\mathrm{m}^{-1}$ and radial density gradients $\lambda_n = 0.1\mathrm{m}$
- 3D slab with uniform magnetic field $B_\varphi = 1\mathrm{T}$

$$\partial_t n + \mathbf{v}_E \cdot \nabla n = \frac{1}{e} \nabla \cdot (j_{\|} \mathbf{b})$$

$$\frac{n m_i}{B^2} \partial_t \nabla_\perp^2 \Phi = \nabla \cdot (j_{\|} \mathbf{b})$$

$$\left(\eta_{\|} + \frac{m_e}{n_e e^2} \partial_t\right) j_{\|} = \frac{T_e}{n} \boldsymbol{\nabla}_{\|} n - \boldsymbol{\nabla}_{\|} \Phi - \partial_t A_{\|}$$

$$\nabla_\perp^2 A_{\|} = -\mu_0 j_{\|}$$

Dispersion relation:

$$i \left(\underbrace{\rho_{L,e}^2 k_\perp^2}_{\text{finite } m_e} + \underbrace{\beta_0}_{\text{induct.}} \right) \omega^3 + \left(- \underbrace{i \beta_0 \omega_*}_{\text{flutter}} - \underbrace{\frac{\eta_{\|} e n_0 T_0 k_\perp^2}{B^2}}_{\text{resistivity}} \right) \omega^2$$

$$- i \omega_s^2 \left(\omega_* - \left(1 + \rho_L^2 k_\perp^2\right) \omega \right) = 0$$

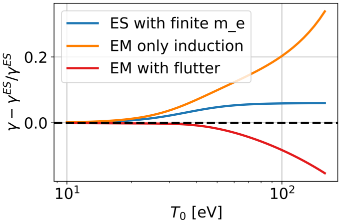

Figure 2: *Change in growth rate of the most unstable mode opposed to the ES model for increasing temperature*

Impact on Drift-Wave Turbulence 1/2

Simulation set-up:

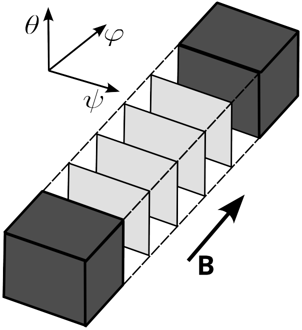

Figure 3: *Scheme of the slab geometry*

- Closed field lines with uniform magnetic field at $B = 1.2$T
- Fixed values for density and temperature on the low-ψ side
  - Excite a drift-wave instability
  - Control β in the system

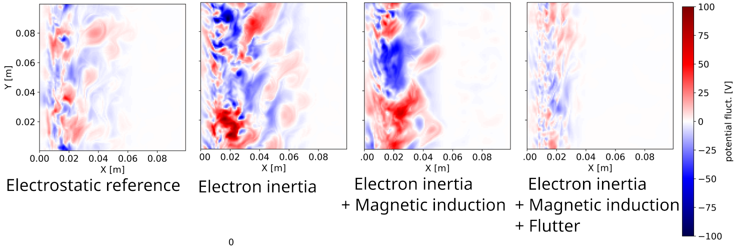

Figure 4: *Potential fluctuations with the ingredients of the EM model*

Width 0.1m×0.1m and length 6m

Discretized in 128 × 128 × 28 cells

Impact on Drift-Wave Turbulence 2/2

Three scenarios with increasing $\beta_{eff} = \beta \left(\frac{L_{\parallel}}{L_{\perp}}\right)^2$:

Profiles averaged over the poloidal direction and time in the saturated turbulence phase

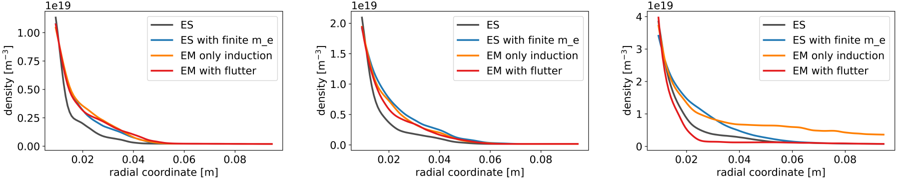

(a) $\beta_{eff} \approx 30$ (b) $\beta_{eff} \approx 90$ (c) $\beta_{eff} \approx 120$

Figure 5: *Averaged radial profiles for density*

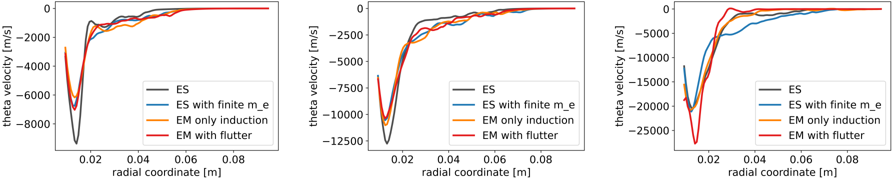

(a) $\beta_{eff} \approx 30$ (b) $\beta_{eff} \approx 90$ (c) $\beta_{eff} \approx 120$

Figure 6: *Averaged velocity in poloidal direction*

Impact on Interchange Instability: 1/2

Same set-up, but includes curvature with a major radius of 2m

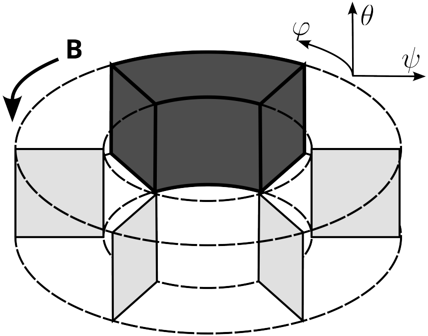

Figure 7: *Scheme of the slab geometry*

- Comparison between the electrostatic reference, electron inertia and the full EM model
- Same prescribed values at the core boundary

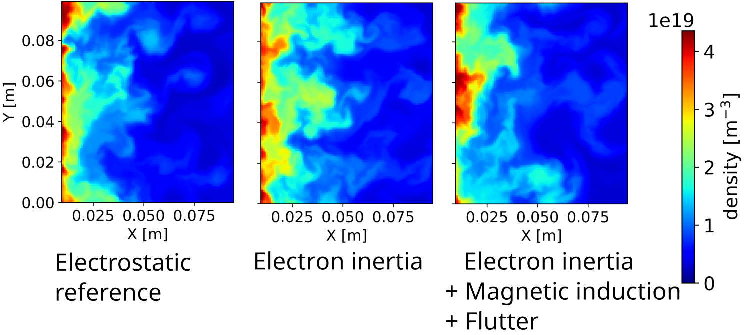

Figure 8: *Density map with the ingredients of the EM model*

Impact on Interchange Instability 2/2

Averaged radial profiles for density : *for three scenarios with increasing* $\beta_{eff} = \beta \left(\frac{L_{\parallel}}{L_{\perp}}\right)^2$:

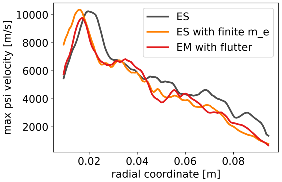

(a) $\beta_{eff} \approx 250$

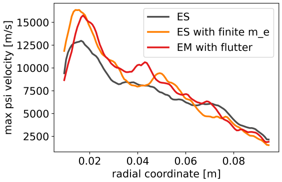

(b) $\beta_{eff} \approx 700$

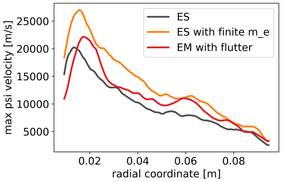

(c) $\beta_{eff} \approx 1100$

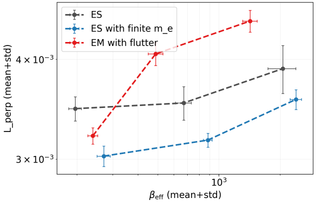

Figure 10: *Estimated $L_{\perp}$ of pressure fluctuations*

Observations

- Electron inertia creates leads to smaller but faster filaments
- At high β, the EM model generates much larger structures that propagate slower

Power Scan on the TCV-X21 Benchmark Case

Simulation of a quarter of a torus with 32 poloidal planes and 2e6 cells

Particle source driven by

fluid neutrals [Quadri et al. 2024]

- Density feedback on the separatrix to $n_{sep} = 7 \cdot 10^{18}$ part/m^3
- Particle recycling 90%, Energy recycling 0%

Compared scenarios

Increasing power influx at the core boundary, equally distributed between electrons and ions

- 150kW (as in TCV-X21)
- 500kW

Comparison between the **electrostatic** and the **full electromagnetic** models
- including electron inertia, magnetic induction and flutter -
Total: 4 simulations

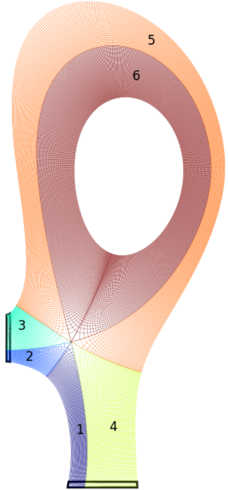

Figure 11: *Discretization of the domain*

Progress of the simulation

- Initial ramp up with `EM 500kW` power
- After 10ms: start of the `EM 150kW` case
- Increase target density at the separatrix to match experimental H-mode conditions

  for `EM 150kW`: $0.7 \cdot 10^{19}\mathrm{m}^{-3}$ for `EM 5 00kW`: $3 \cdot 10^{19}\mathrm{m}^{-3}$
- Start electrostatic scenarios from available profiles
- Recently: Restore target density $0.7 \cdot 10^{19}\mathrm{m}^{-3}$ for all cases

PROFILES NOT (YET) CONVERGED!!

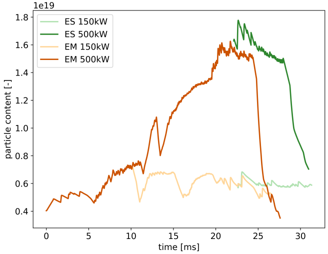

(a) Total particle content

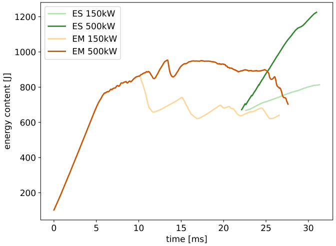

(b) Total energy content

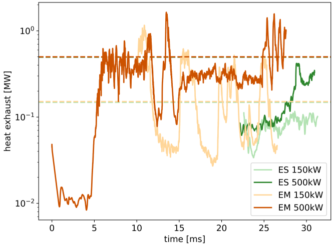

(c) Total energy in/out-flow

Global plasma profiles

Profiles at the outer midplane after resetting the density

- Toroidal averages over all poloidal planes
- Temporal averages over the last available 30μs

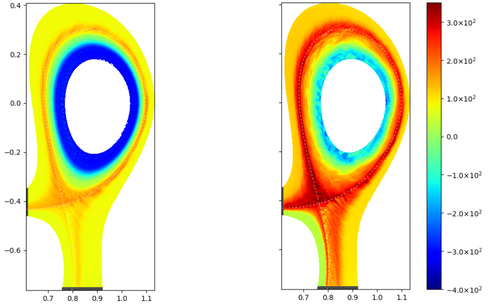

(a) ES - 500kW (b) EM - 500kW

Figure 13: 2D map of the electric potential Φ

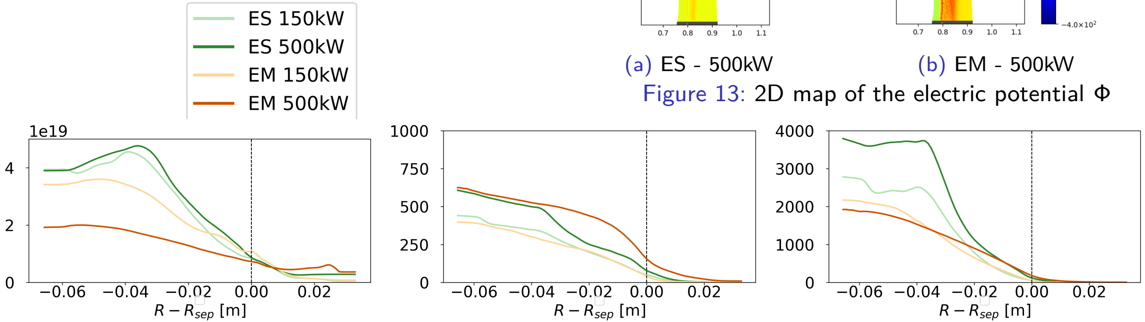

(a) Density [m^{-3}] (b) Electron temperature [eV] (c) Electron pressure [Pa]

Figure 14: Mean profiles at the outer-mid plane

Characteristics of radial heat transport

- At **low power**: similar radial energy fluxes and turbulence levels across the mid-plane
- At **high power**: Stronger increase in turbulence and consequent radial heat transport with the electromagnetic model

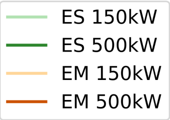

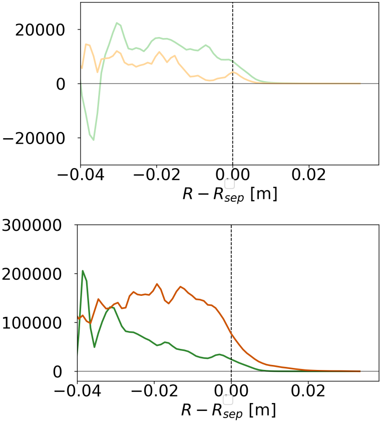

Figure 15: Radial energy flux for electrons [Wm^{-2}]

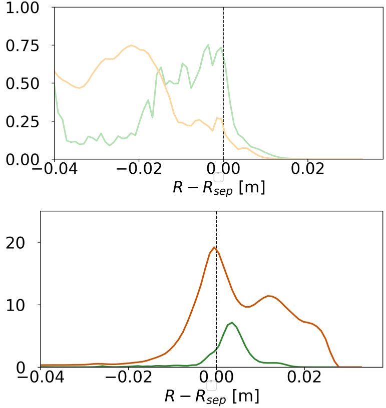

Figure 16: Turbulent ExB kinetic energy [Jm^{-3}]

Magnetic flutter field

- **Expectation**: the amplitude of the flutter field scales with the plasma β

- **Reality**: at higher power, the flutter field is considerably stronger

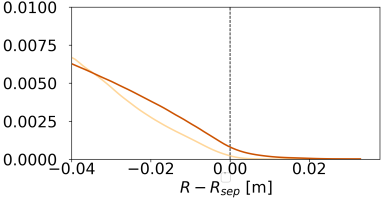

(a) $\beta = \frac{p}{p_{mag}} = \frac{enT}{B^2/(2\mu_0)}$

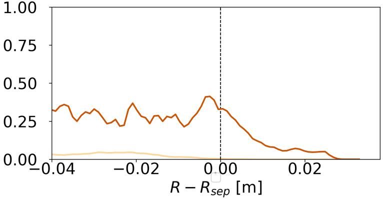

(b) Energy for field line bending [Jm^{-3}]

$$\mathcal{E}_{mag} = \frac{B_{pert}^2}{2\mu_0}$$

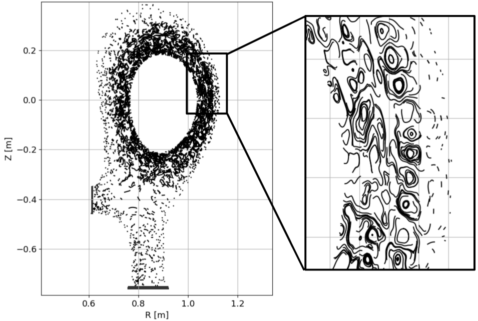

Figure 18: Traced field lines of the flutter field $\mathbf{B}_{pert}$

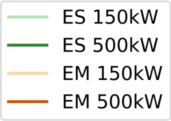

A dive into turbulent structures

As power increases, the EM model develops **larger**, more **energetic** filaments

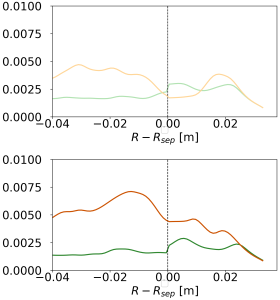

Figure 19: Estimated perpendicular structure sizes [m]

$$L_\perp = \sqrt{\frac{\langle \tilde{p}_e \rangle_\varphi}{|\nabla_\perp \tilde{p}_e|}}$$

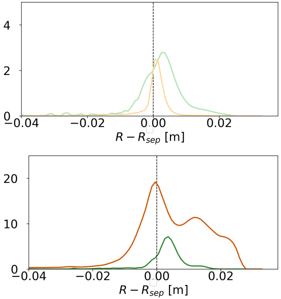

Figure 20: Turbulent energy of temperature fluctuations [Jm^{-3}]

$$\mathcal{E}_{\mathrm{T,fluct}} = \sum_{i,e} \frac{3}{2} \frac{e \langle n \rangle_\varphi}{\langle T \rangle_\varphi} |\tilde{T}|^2$$

with $\tilde{X} = X - \langle X \rangle$

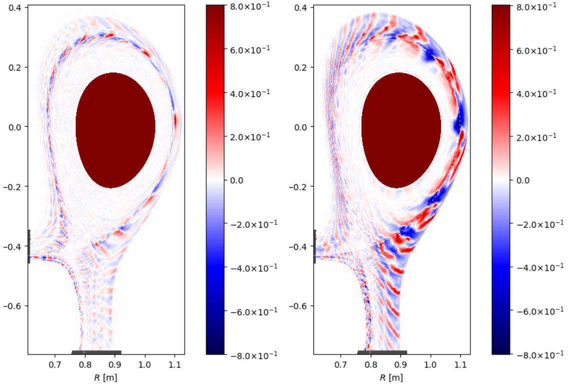

(a) Electrostatic (b) Electromagnetic

Figure 21: Relative electron pressure fluctuations for the 500kW scenario

Instability drive

Turbulence suppression due to shear occurs as the electric shear γ_E exceeds the linear fluctuation growth rate $\gamma_\star$

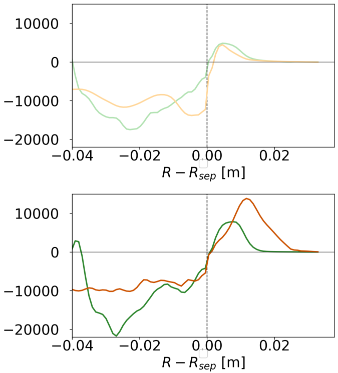

Figure 22: Radial electric field E_r [Vm^{-1}]

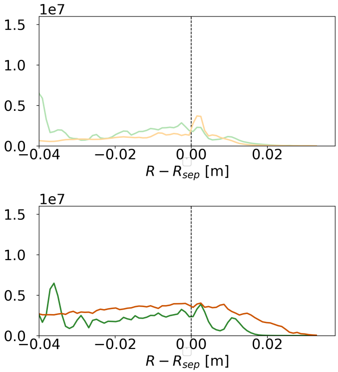

Figure 23: Electric shear [s^{-1}]
$\gamma_E = \left| \frac{\partial}{\partial r} \left(\frac{E_r}{B} \right) \right|$

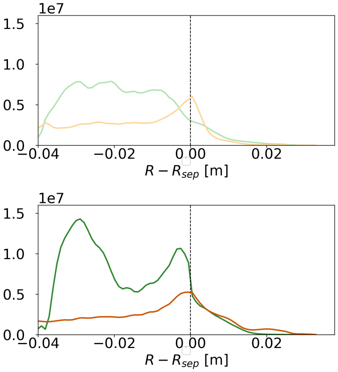

Figure 24: Linear growth [s^{-1}]
$\gamma_\star = C \frac{k_\perp |\nabla p|}{enB}$

Conclusion

Electromagnetic model

- Magnetic induction in the parallel electric field
- Fluctuations of the equilbrium magnetic field with flutter
- Electron inertia to constrain Alfvén wave speeds and for numerical stability

Observations

- Destabilizing effect of electron inertia and magnetic induction
- Stabilizing effect of flutter
- Larger plasma blobs and further propagation with the EM model at high power

Set of simulations

- Study of drift-wave and interchange instabilities on a slab geometry
- TCV simulations to compare the ES and EM model under two power regimes

Outlook

- Continue the TCV simulations until to reach a quasi steady-state
- Investigate the radial electric field and the L-H transition on slab cases